Supporting Information

Silicon Solar Cell-Enabled Organic Photoelectrochemical Transistor Optoelectronics

Yi-Tong Xu[1], Cheng Yuan[1], Bing-Yu Zhou[1], Zheng Li[1], Jin Hu[2], Peng Lin[2], Wei-Wei Zhao[1*], Hong-Yuan Chen[1], Jing-Juan Xu[1*]

[1]State Key Laboratory of Analytical Chemistry for Life Science, School of Chemistry and Chemical Engineering, Nanjing University, Nanjing 210023, China

[2]Shenzhen Key Laboratory of Special Functional Materials & Guangdong Research Center for Interfacial Engineering of Functional Materials, College of Materials Science and Engineering, Shenzhen University, Shenzhen 518060, China

*Corresponding author. E-mail: zww@nju.edu.cn; xujj@nju.edu.cn

PEDOT:PSS polymer was used as the channel material for the depletion mode OECT device. As shown in Fig. S1, PEDOT is a semiconductor initially in high conductance state with holes as the main carrier [1], which is originated from inductive effect by the negative-charged sulfonate moieties of the PSS. The increasing anodic V_{gs} would facilitate cations' injection from electrolyte into the polymer film, resulting in the compensation of negative charges, depletion of holes, and decrease of channel conductance. The opposite is true for the increase of cathodic V_{gs}.

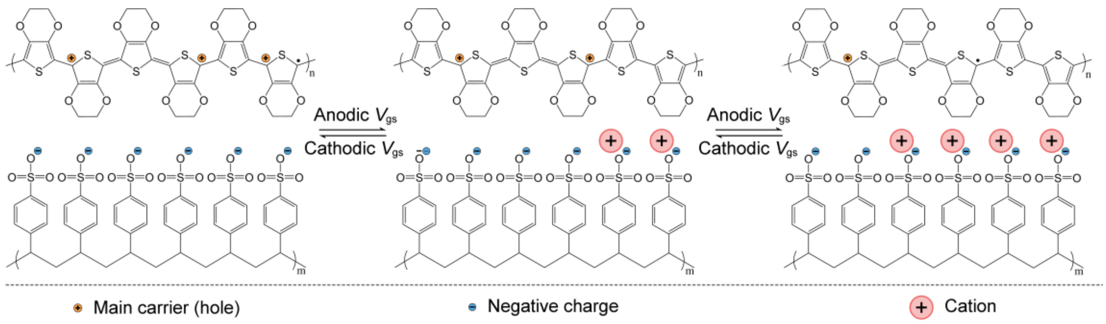

Figure S1 Molecular structure of the PEDOT:PSS polymer for depletion-mode OECT and working rationale.

Depletion-mode OECT characteristics in the first quadrant were studied. Fig. S2 a1 illustrates the diagram of the OECT powered by two instrumental suppliers. Fig. S2 a2 shows the corresponding output characteristics. Fig. S2 a3 shows the transfer characteristics recorded by scaning V_{gs} at varied positive V_{ds}. At a fixed V_{ds}, the absolute value of I_{ds} exhibited gradual decrease with the increase of V_{gs}, while the transfer curves shifted to higher positive I_{ds} with the increase of V_{ds} from +0.01 V to +0.30 V. As shown in Fig. S2 a4, as V_{ds} became more positive, the maximal transconductance exhibited stepwise increase from 0.32, 1.20, 2.99, 5.21, to 8.16 mS, with the corresponding positive shift of V_{gs} from 0.102, 0.108, 0.135, 0.170, to 0.223 V.

As illustrated in Fig. S2 b1, the d-s instrumental power supplier was then substituted by the MSSC, with the opposite poles compared to Fig. 1 b1. As shown in Fig. S2 b2, the corresponding output characteristics were obtained by continuously increasing L_{ds} under different V_{gs}. The I_{ds} values was increased with larger slopes at the begining and with smaller slopes at larger L_{ds}, but still did not enter constant current mode. Fig. S2 b3 shows the corresponding transfer characteristics. Upon the light illumination, the device could be turned on and entered a constant-current mode until a specific threshold V_{gs} that could turn off the device. With the increase of L_{ds}, the I_{ds} became more positive, and the threshold V_{gs} moved to lower values, but with larger amplititudes compared to Fig. 1 b3. As shown in Fig. S2 b4, the transconductances grew larger with the increase of L_{ds}, with the maximal transconductances moved to lower V_{gs}. Note that at similar I_{ds} levels, smaller transconductances were aquired in this case as compared to Fig. 1 b4, but larger when compared to Fig. S2 a4.

Next, as illustrated in Fig. S2 c1, the g-s instrumental power supplier was substituted by the MSSC. Fig. S2 c2 shows the corresponding output characteristics. As the increase of L_{gs} from 0.00 mW cm^{-2} to 1.08 mW cm^{-2}, I_{ds} exhibited stepwise decrease. Fig. S2 c3 shows the corresponding transfer characteristics. The transfer curves shifted to higher I_{ds} with increase of V_{ds} from +0.01 V to +0.30 V, while the I_{ds} started to be inhibited until 2 mW cm^{-2} and could not be completely shut off even at 20 mW cm^{-2}. As shown in Fig. S2 c4, as the V_{ds} changed from +0.01 V to +0.30 V, five transconductance peaks of 0.001, 0.124, 0.288, 0.492, to 0.774 mA/(mW cm^{-2}) appeared at the same L_{gs} of 3.42 mW cm^{-2} on the curves.

As illustrated in Fig. S2 d1, both the g-s and d-s instrumental power suppliers were then substituted by the MSSCs with individual light illumination. As shown in Fig. S2 d2, the corresponding output characteristics were measured by continuously increasing L_{ds} under different L_{gs}. The curves exhibited larger slopes at lower L_{ds}, turned smaller at higher L_{ds}, and the I_{ds} values did not tend to be constant. As shown in Fig. S2 d3, the transfer characteristics were obtained by continuously increasing L_{gs} under different L_{ds}. Upon the application of L_{ds}, the device could be turned on, but the I_{ds} seemed not to be shut off even L_{gs} came to 50 mW cm^{-2}. The corresponding transconductances were derived as shown in Fig. S2 d4. The peak transconductances and corresponding L_{gs} were adjustable dependent upon the variant L_{ds}, but only smaller maximal transconductances could be obtained and larger L_{gs} was needed.

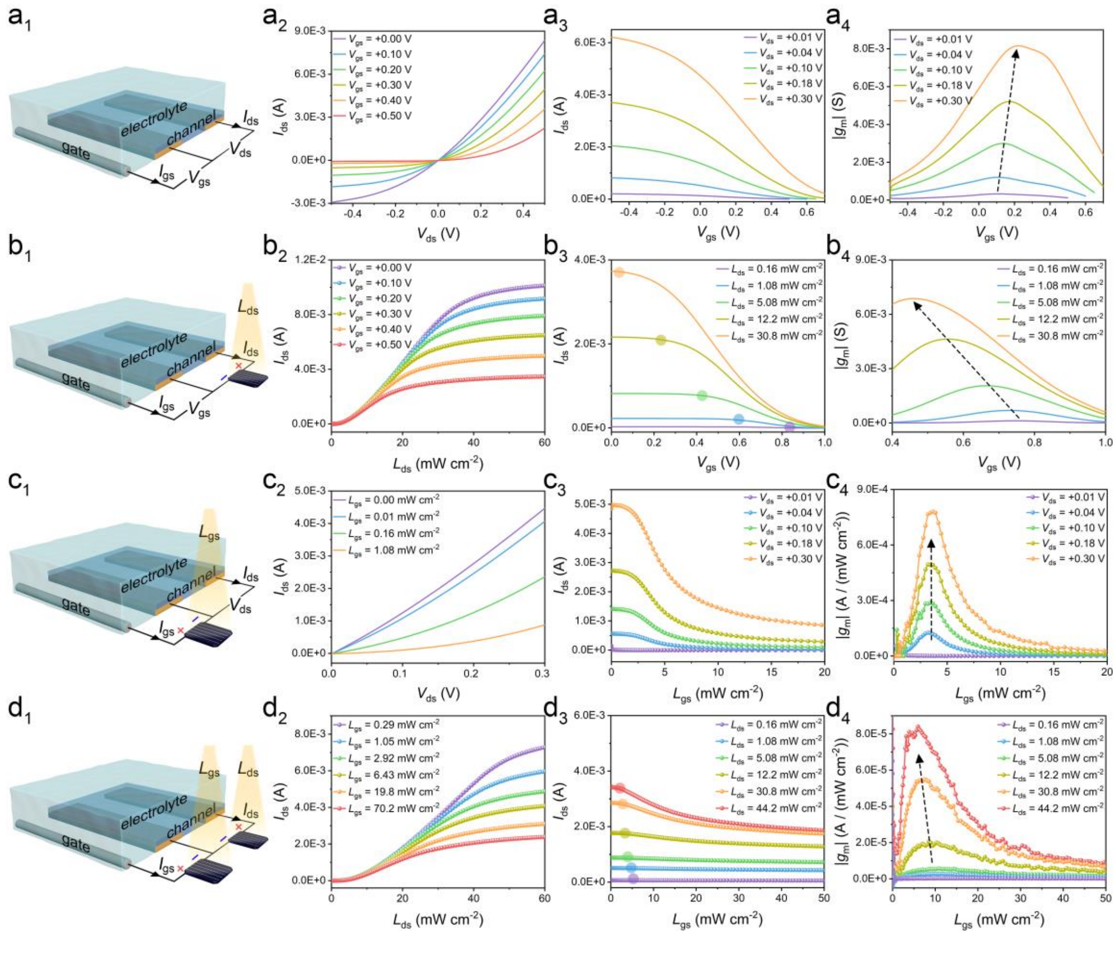

Figure S2 Schematic of MSSC-enabled depletion-mode OECT and characteristics in the first quadrant. (a1-d1) represent OECT devices powered by two instrumental suppliers, MSSC for d-s, g-s, and both circuits, respectively. The arrows indicate positive flow of the current. (a2-d2), (a3-d3), and (a4-d4) represent corresponding output, transfer characteristics, and transconductance evolution of the systems.

To ensure the capability of the MSSC to power the OECT circuits, we have studied the photovoltaic properties of the MSSC at variant irradiances up to 100 mW cm^{-2} (AM 1.5 sunlight conditions). As shown in Fig. S3a, with the increase of voltage, the curves went down and intersected with the *x* axis, where the voltage of intersection points were denoted as open-circuit potential (V_{OC}). With the irradiance increasing, the current density was stepwisely kept at larger value up to 58.72 mA cm^{-2}, and V_{OC} up to 0.578 V. Fig. S3b shows the corresponding output power-voltage curves. With the irradiance increasing, the output power of the MSSC could reach ca. 6 mW, which was sufficient to power either d-s circuit (within several mWs, from the output characteristics) or g-s circuit (much smaller than the d-s circuit). As shown in Fig. S3c-d, the short-circuit current density and open-circuit potential shows a linear relationship toward irradiance and logarithmic irradiance, respectively.

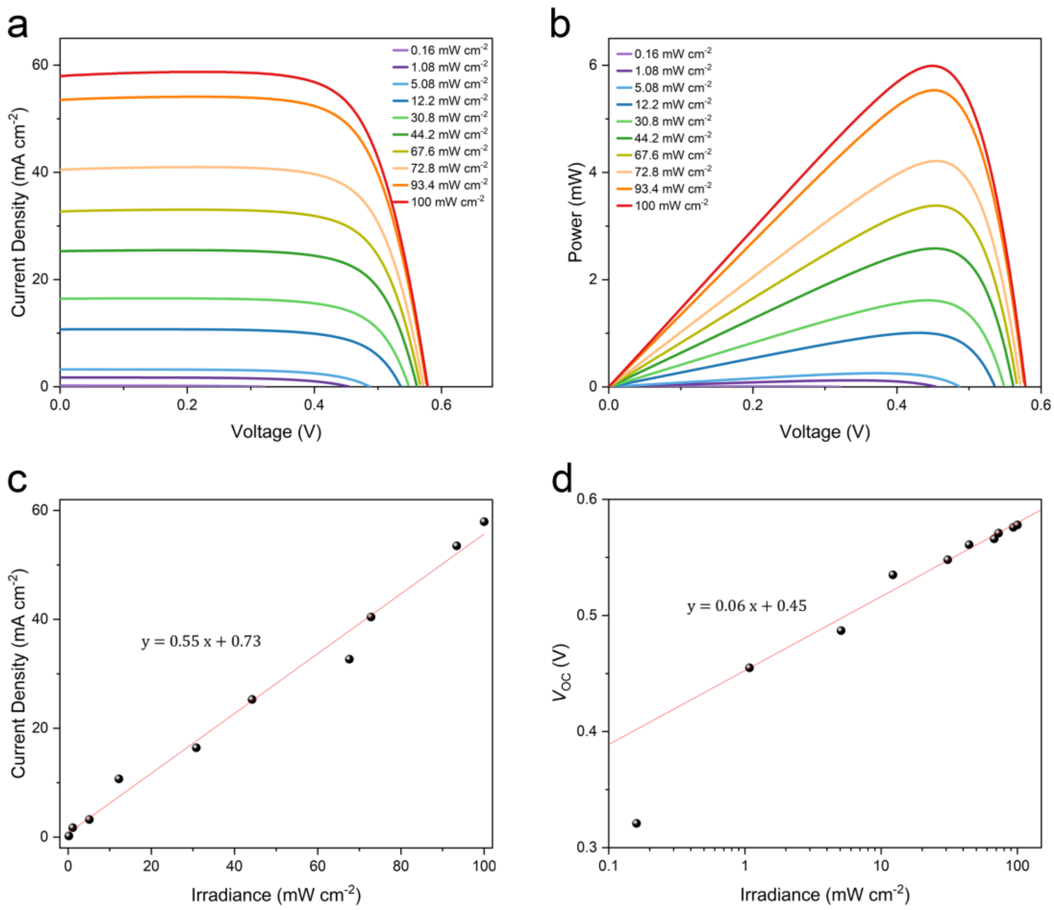

Figure S3 Photovoltaic properties of the MSSC. a-b) *J-V* and *P-V* curves at different irradiances. c-d) Derived short-circuit current density and open-circuit potential as functions toward irradiance.

As shown in Fig. S4, the doping/de-doping, oxidation/reduction mechanisms of the accumulation-mode OECT were similar to the depletion-mode OECT, whereas the PEDOT:PSS polymer film of accumulation-mode OECT channel was doped with positive-charged oxidized amine molecules (R-NH_2) that would naturally compensate negative-charged sulfonate moieties of the PSS, leading to fewer holes in the PEDOT polymer and diminished I_{ds}.

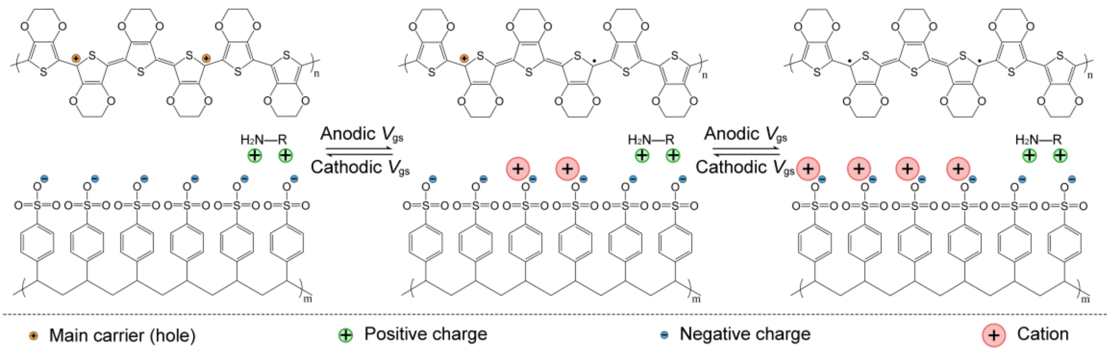

Figure S4 Molecular structure of the DETA de-doped PEDOT:PSS polymer for accumlation-mode OECT and working rationale.

Accumulation-mode OECT characteristics in the first quadrant were studied. Fig. S5 a1 illustrates the diagram of the OECT powered by two instrumental suppliers. Fig. S5 a2 shows the corresponding output characteristics. Fig. S5 a3 shows the transfer characteristics recorded by scaning V_{gs} at varied positive V_{ds}. At a fixed V_{ds}, the absolute value of I_{ds} exhibited gradual increase with the decrease of V_{gs}, while the transfer curves shifted to higher positive with the increase of V_{ds} from +0.01 V to +0.18 V. As shown in Fig. S5 a4, as V_{ds} became more positive, the maximal transconductance exhibited stepwise increase from 0.73, 3.01, 7.62 to 13.16 mS, with the general positive shift of V_{gs} from -0.316, -0.309, -0.335 to -0.222 V.

As illustrated in Fig. S5 b1, the d-s instrumental power supplier was then substituted by the MSSC, with the opposite poles compared to Fig. 2 b1. As shown in Fig. S5 b2, the corresponding output characteristics were obtained by continuously increasing L_{ds} under different V_{gs}. The I_{ds} values was increased with increase of L_{ds} and decrease of V_{gs}, and tended to be overlapped after V_{gs} of 0.0 V. Fig. S5 b3 shows the corresponding transfer characteristics. Upon the light illumination, the I_{ds} was kept in the off state, then increased to positive value with V_{gs} decreasing until a specific threshold V_{gs} that could keep the I_{ds} on. As shown in Fig. S5 b4, the transconductances grew larger with the increase of L_{ds}, with the maximal transconductances moved to lower V_{gs}.

Next, as illustrated in Fig. S5 c1, the g-s instrumental power supplier was substituted by the MSSC. Fig. S5 c2 shows the corresponding output characteristics. As the increase of L_{gs} from 0.00 mW cm^{-2} to 1.05 mW cm^{-2}, I_{ds} exhibited stepwise increase, with different but nearly constant rates. Fig. S5 c3 shows the corresponding transfer characteristics. The transfer curves shifted to higher I_{ds} with increase of V_{ds} from +0.01 V to +0.18 V, while the increased L_{gs} could further boost the I_{ds} signals. In this case, L_{gs} within 0.50 mW cm^{-2} could start to turn on the device. As shown in Fig. S5 c4, as the V_{ds} changed from +0.01 V to +0.18 V, four transconductance peaks of 0.21, 0.83, 2.14, to 4.06 mA/(mW cm^{-2}) appeared at the same L_{gs} of 0.33 mW cm^{-2} on the curves.

As illustrated in Fig. S5 d1, both the g-s and d-s instrumental power suppliers were then substituted by the MSSCs with individual light illumination. As shown in Fig. S5 d2, the corresponding output characteristics were measured by continuously increasing L_{ds} under different L_{gs}. With increase of L_{gs}, the curves at different L_{ds} were overlapped, and showed little variance even when the L_{gs} was larger than 50 mW cm^{-2}, suggesting the poor modulation ability of the L_{gs} to this system. As shown in Fig. S5 d3, the transfer characteristics were obtained by continuously increasing L_{gs} under different L_{ds}. Upon the application of varied L_{ds}, the device started to work with the I_{ds} stationed at the different levels. With L_{gs} increasing, the I_{ds} increased to a more positive value but with limited amplitudes. The corresponding transconductances were derived as shown in Fig. S5 d4. The peak transconductances and corresponding L_{gs} were adjustable dependent upon the variant L_{ds}, but with much smaller maximal transconductances and larger L_{gs} as compared to Fig. S5 c4.

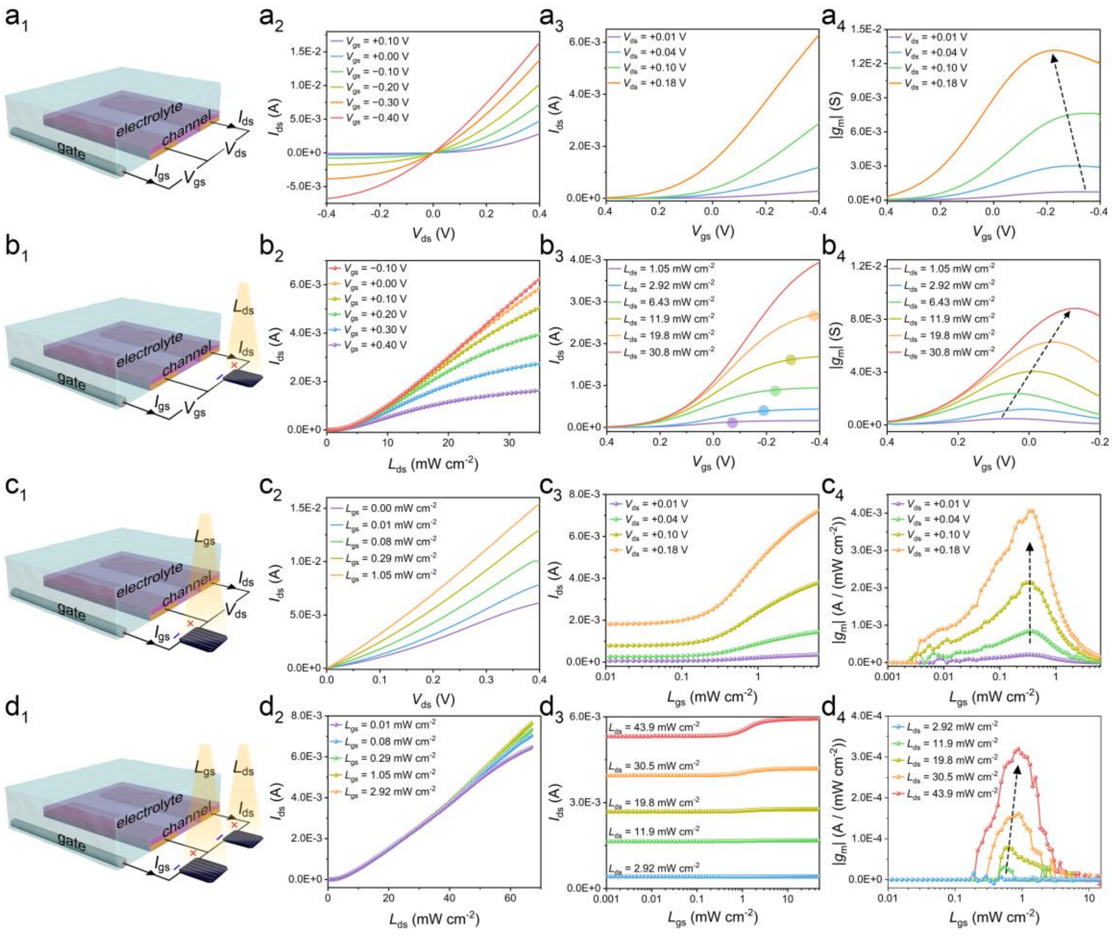

Figure S5 Schematic of MSSC-enabled accumulation-mode OECT and characteristics in the first quadrant. (a1-d1) represent OECT devices powered by two instrumental suppliers, MSSC for d-s, g-s, and both circuits, respectively. (a2-d2), (a3-d3), and (a4-d4) represent corresponding output, transfer characteristics, and transconductance evolution of the systems.

References

[1] Rivnay J, Inal S, Salleo A, et al. Organic electrochemical transistors. Nat Rev Mater, 2018, 3: 17086.